Risk-Averse Trajectory Optimization for a Snake-Inspired Robot

I. Problem definition

We apply the proposed approach on a more complex problem inspired from the EELS robotics mission concept [1], see Figure 2. The problem consists of trajectory optimization for a snake-inspired robotic system [2] navigating in a vent on Enceladus. High-levels of uncertainty are present in the form of external disturbances forces from the plume and uncertain friction coefficients due to uncertain properties of the vent. We are not aware of prior work on uncertainty-aware contact-implicit trajectory optimization for this system.

A. Robot and vent environment parameterization

The snake-inspired robot consists of $N = 10$ identical connected components that are each equiped with an Archimedes' screw allowing longitudinal motion in the vent, see [2] for a description of the system. We consider a cylindrical vent, such that each one of the N joints located at length $\ell \in [0, L]$ and time $t \in [0, T]$ is parameterized by

$$p_\ell(t) = (z_\ell(t), \theta_\ell(t)) \in \mathbb{R}^2 \tag{1}$$

where z_ℓ is its height in the vent and θ_ℓ its angle, and its corresponding 3d position in the vent is given by

$$P_\ell(t) = (r\cos(\theta_\ell(t)), r\sin(\theta_\ell(t)), z_\ell(t)) \in \mathbb{R}^3. \tag{2}$$

where r is the radius of the cylindrical vent, which we take as a constant for simplicity. In addition, the head of the robot consists of an additional joint that allows orienting the robot in the vent. We thus describe the state of the system with

$$x(t) = (p_0(t), \dots, p_{(N-1)\Delta L}(t), p_L(t), \varphi_L(t)) \in \mathbb{R}^{2N+3}$$

where $\Delta L = L/N$ and φ_L is the orientation of the robot's head relative to the horizontal plane of the cylindrical vent, see Figure 1.

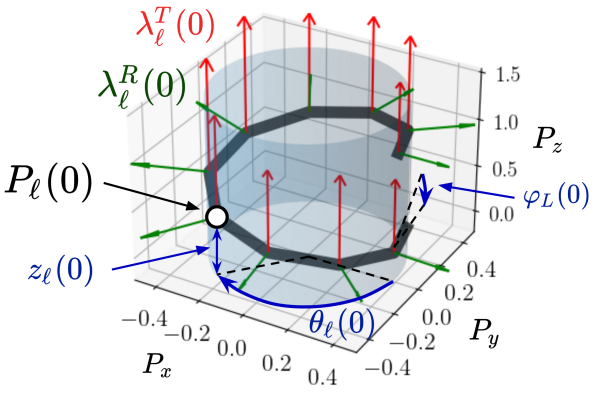

Fig. 1: Variables defining the problem. Initial state of the system.

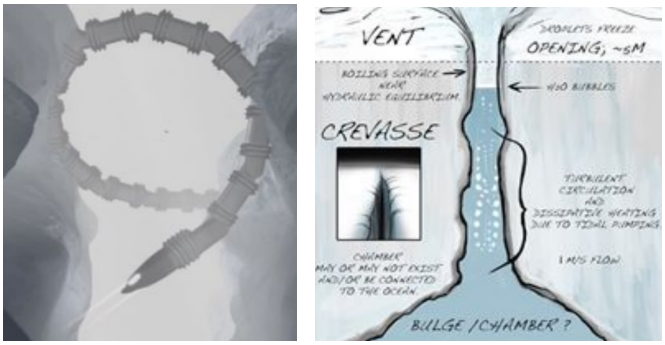

Fig. 2: EELS robotic mission concept. Figures from [1].

We opt for a contact-implicit problem formulation. Thus, the control inputs of the system contain the contact forces

$$\lambda_\ell(t) = (\lambda_\ell^T(t), \lambda_\ell^R(t)) \in \mathbb{R}^2 \tag{3}$$

between the robot and the vent at length ℓ and time t, where $\lambda_\ell^T(t)$ corresponds to tangential contact forces in the vertical direction of the vent, and $\lambda_\ell^R(t)$ corresponds to normal forces along the radial axis of the cylindrical vent, see Figure 1. Let $\Delta\varphi_L$ be the direction change of the robot's head. With this parameterization, the control input is the concatenation of the contact forces $\lambda = (\bar{\lambda}_\ell^T, \lambda_\ell^R)_{\ell\in[0,T]}$ and the change in direction $\Delta\varphi_L$:

$$u(t) = (\lambda_0(t) \dots, \lambda_{(N-1)\Delta L}(t), \lambda_L(t), \Delta\varphi_L(t)) \in \mathbb{R}^{2N+3}.$$

By only considering screw-propelled longitudinal forward motion in the vent (see [2] for details on possible locomotion modes of this robot), the time-evolution of the system can be described by the dynamics constraints

$$p_{k\Delta L}(t+\Delta t) = p_{(k+1)\Delta L}(t+\Delta t),\ k=0,\dots,N-1, \tag{4a}$$

$$p_L(t+\Delta t) = \begin{bmatrix}\Delta L\sin(\varphi_L(t))\\ \Delta L\cos(\varphi_L(t))\end{bmatrix}, \tag{4b}$$

$$\varphi_L(t+\Delta t) = \varphi_L(t) + \Delta\varphi_L(t), \tag{4c}$$

where $\Delta t = L/v$ with $v > 0$ the longitudinal robot speed. Although this problem is not formulated in continuous-time, the analysis and results in the main paper (see Theorem 1) apply to this discrete-time formulation[1]. We do not consider stochasticity in the dynamics in this scenario since the main source of uncertainty comes from external disturbance forces from the plume and friction coefficients in the vent.

[1]Continuous-time SDE formulations yield functions that are only α-Hölder continuous for $\alpha \in (0, 1)$, which requires using non-classical concentration inequalities to derive Theorem 1, see the main paper and `errorbound.pdf` for details on concentration inequalities. In particular, thanks to (4), all functions defined in this supplementary document are Lipschitz continuous, and thus they are in particular α-Hölder continuous.

B. Sources of uncertainty

The main sources of uncertainty come from external disturbance forces $F_\ell(t)$ from the plume and friction coefficients in the vent $\mu(p_\ell(t))$. We model the plume forces $F_\ell(t)$ as uniformly distributed. We consider a friction coefficient that is uncertain at a given height $\bar{z}$ and at $\bar{\theta} = 0$. The uncertain space-varying friction coefficient then satisfies

$$\mu(p_\ell(t), \omega) = \bar{\mu} + \omega \Psi \left(\frac{z_\ell(t) - \bar{z}}{100} + 10 \sin(\theta_\ell(t)/2) \right) \quad (5)$$

where $\Psi : \mathbb{R} \to \mathbb{R}$ is a bump function defined by $\Psi(y) = \exp\left(2 - 2/(1-y^2)\right)$ if $y \in (-1, 1)$ and 0 otherwise, $\bar{\mu} > 0$ is a nominal friction coefficient, and ω is uniformly-distributed. We represent $\mu(p_\ell(t), \omega)$ in Figure 3.

C. Equilibrium constraint

The robot should never fall while descending the vent. This requirement can be encoded as the three following *static equilibrium* constraints

$$\sum_{k=0}^{N+1} \lambda^R_{k\Delta L}(t) \cos(\theta_{k\Delta L}(t)) = 0 \quad (6)$$

$$\sum_{k=0}^{N+1} \lambda^R_{k\Delta L}(t) \sin(\theta_{k\Delta L}(t)) = 0 \quad (7)$$

$$\sum_{k=0}^{N+1} \left(\lambda^T_{k\Delta L}(t) + F_\ell(t) \right) = 0 \quad (8)$$

that should hold with $\mathbb{P}$-probability one (over the uncertain friction coefficients and the disturbance forces) for all times t. In (6)-(8), we assume that the disturbance forces from the plume only act vertically, such that disturbance forces only affect the tangential contact force components in (8). Thus, to enforce these force balance constraints, we specify the feedback law in the tangential direction

$$\lambda^T_\ell(t) = \bar{\lambda}^T_\ell(t) - K(\omega, t) \mu_\ell(p_\ell(t)) F_\ell(\omega, t) \quad (9)$$

where $\mu_\ell(p_\ell(t)) \in \mathbb{R}$ is the friction coefficient at position $p_\ell(t)$ and K is a feedback gain. By manipulating (8), we obtain that the feedback gain must satisfy

$$K(\omega, t) = \frac{\sum_{k=0}^{N+1} \left(\bar{\lambda}^T_{k\Delta L}(t) + F_{k\Delta L}(\omega, t) \right)}{\sum_{k=0}^{N+1} \mu_{k\Delta L}(p_{k\Delta L}(t)) F_{k\Delta L}(\omega, t)}. \quad (10)$$

D. Contact force constraints and friction limits

Additional constraints are imposed on contact forces. First, the robot can only push against the vents, i.e., *normal forces are non-negative* (and bounded to satisfy hardware limits):

$$0 \leq \lambda^R_\ell(t) \leq \bar{\lambda}^R_\ell(t) \quad \forall \ell, \ \forall t. \quad (11)$$

This constraint corresponds to a standard bounded control constraint. To enforce *friction limits*, we also impose the no-slip constraint at risk-level α:

$$\text{AV@R}_\alpha \left(\sup_{\ell \in [0,L]} \sup_{t \in [0,T]} \left(\lambda^T_\ell - \mu(p_\ell) \lambda^R_\ell(t) \right) \right) \leq 0. \quad (12)$$

Note that the contact force $\lambda^T_\ell =$ (9) and friction coefficient $\mu(p_\ell)$ in (12) are uncertain, which motivates using a risk-constrained problem formulation. The stochasticity in this constraints appears from the dependency on the state of the system and the effect of force feedback in (9).

E. Cost function

With the goal of accessing the ocean water below the ice shell of Enceladus [1], we formulate the objective as

$$\inf_u \quad z_L(T) \quad (13)$$

which corresponds to reaching the lowest possible altitude z_L at the end of the planning episode. The initial condition of the system with $z_L(0) = 0$ is shown in Figure 1.

II. Results

By combining the constraints (4)-(12) and using the objective in (13), we obtain a risk-constrained planning problem taking the form of **OCP** as defined in the main paper. This allows us to apply the proposed approach to solve this problem. We discretize the problem with $S = 20$ timesteps and approximate the constraints with $M = 10$ samples using the proposed sample average approximation approach.

We compare with a baseline that does not consider variability in the friction coefficient and external forces (i.e., μ and F are constant). We present results in Figure 3. Although the baseline trajectory quickly traverses the vent and reaches a final height of $z_L(T) = -5.25\,\text{m}$, it almost always violates the no-slip constraints. In contrast, the trajectory obtained with the proposed approach achieves a more conservative final height of $z_L(T) = -2.35\,\text{m}$ and satisfies all constraints $75.6\,\%$ of the time. To conclude, considering risk in this scenario leads to a safer trajectory that allows traversing the vent while reducing the risk of slippage.

References

[1] K. Carpenter, M. Cable, M. L.and Choukrouny, H. Ono, R. Thakker, M. Ingham, P. McGarey, A. Barchowski, S. Iacoponi, J. Bowkett, W. Reid, and E. Marteou. Venture deep, the path of least resistance: Crevasse-based ocean access without the need to dig or drill. In *Bulletin of the American Astronomical Society*, 2021.

[2] D. A. Schreiber, F. Richter, A. Bilan, P. V. Gavrilov, H. M. Lam, C. H. Price, K. C. Carpenter, and M. C. Yip. ARCSnake: An Archimedes' screw-propelled, reconfigurable serpentine robot for complex environments. In *Proc. IEEE Conf. on Robotics and Automation*, 2020.

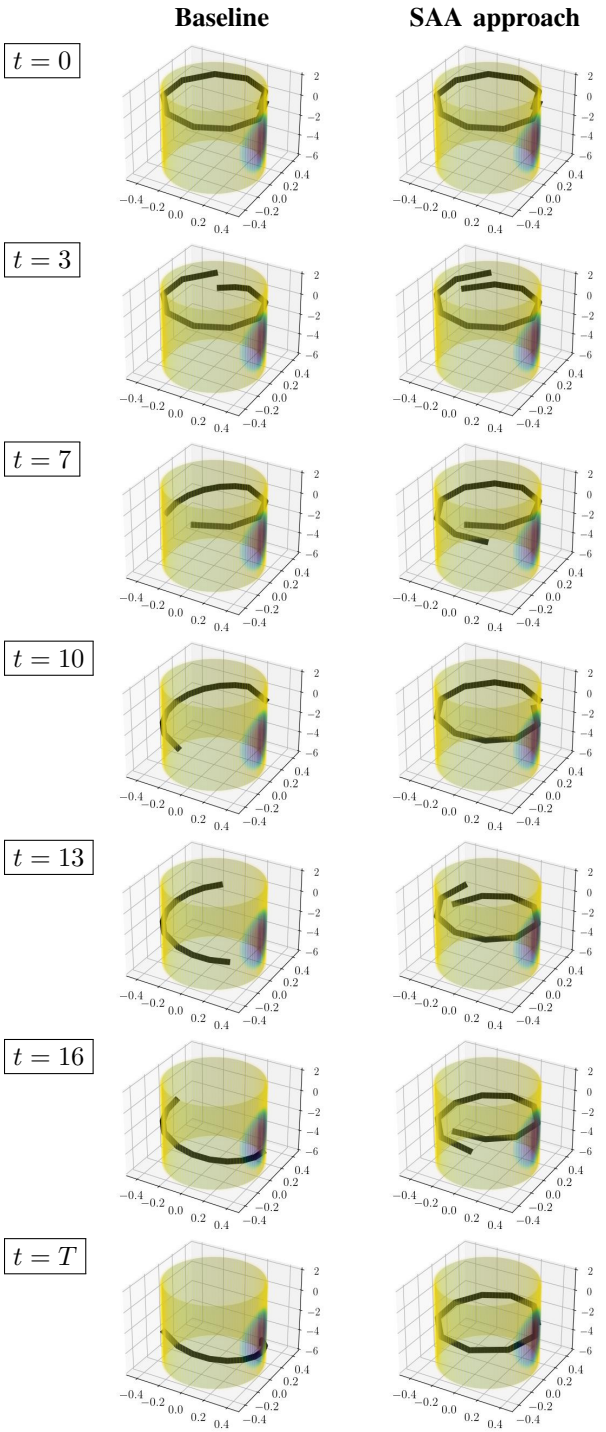

Fig. 3: Left: trajectory obtained using the baseline. Right: trajectory obtained with the proposed risk-sensitive approach.